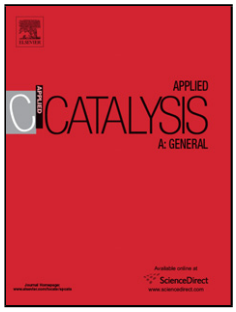

Title: Fast and Facile Preparation of Metal-doped g-C_3N_4 Composites for Catalytic Synthesis of Dimethyl Carbonate

Author: Jie Xu Kai-Zhou Long Yue Wang Bing Xue Yong-Xin Li

PII: S0926-860X(15)00117-9
DOI: http://dx.doi.org/doi:10.1016/j.apcata.2015.02.025
Reference: APCATA 15262

To appear in: *Applied Catalysis A: General*

Received date: 3-12-2014
Revised date: 3-2-2015
Accepted date: 13-2-2015

Please cite this article as: J. Xu, K.-Z. Long, Y. Wang, B. Xue, Y.-X.L. Fast and Facile Preparation of Metal-doped g-C_3N_4 Composites for Catalytic Synthesis of Dimethyl Carbonate, *Applied Catalysis A, General* (2015), http://dx.doi.org/10.1016/j.apcata.2015.02.025

Highlights

- Metal-doped g-C_3N_4 samples were prepared via a simple mixing and calcination.
- No hard template or etching was required in the synthesis of doped g-C_3N_4.
- A maximum DMC yield of 83.3% was obtained over Zn-g-C_3N_4 material.
- Doped g-C_3N_4 showed superior activity to other mesoporous carbon nitrides.

Graphical Abstract

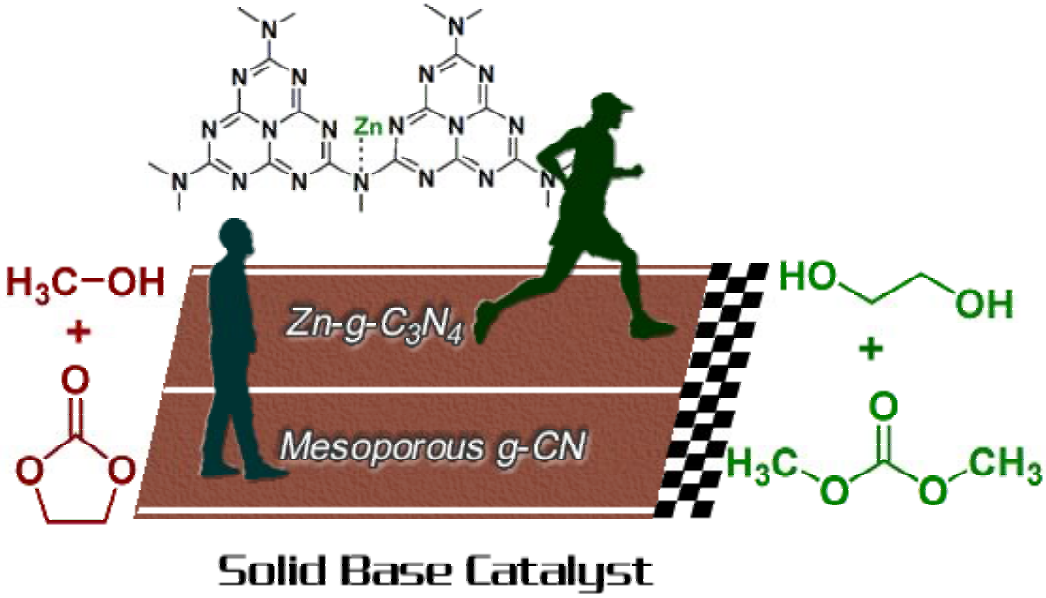

Manuscript title:

Fast and Facile Preparation of Metal-doped g-C_3N_4 Composites for Catalytic Synthesis of Dimethyl Carbonate

Authors' names:

Jie Xu *, Kai-Zhou Long, Yue Wang, Bing Xue, Yong-Xin Li *

Authors' affiliation:

Jiangsu Key Laboratory of Advanced Catalytic Materials and Technology, School of Petrochemical Engineering, Changzhou University, Gehu Road 1, Changzhou, Jiangsu 213164, PR China

Corresponding authors:

Dr. Jie Xu

Tel.: +86-519-86330135; E-mail: shine6832@163.com

Prof. Yong-Xin Li

Tel.: +86-519-86330135; E-mail: liyxluck@163.com

Abstract:

Zn-doped g-C_3N_4 materials (Zn-g-C_3N_4) were prepared by a simple mixing and calcination, using dicyandiamide as a precursor and zinc halide as a dopant. The characterization results of CO_2 temperature-programmed desorption and elemental analysis revealed that the introduction of Zn species enhanced the overall basic quantity of g-C_3N_4. In the transesterification of ethylene carbonate with CH_3OH to dimethyl carbonate (DMC), the Zn-g-C_3N_4 catalysts showed superior catalytic activity to the pure g-C_3N_4, and the highest DMC yield reached 83.3%, along with stable catalytic reusability and reproducibility. Furthermore, other transition-metal halides (including $FeCl_3$, $CuCl_2$, $NiCl_2$, etc) could be utilized as dopants for g-C_3N_4, and the obtained doped g-C_3N_4 materials also showed high EC conversions above 70%. The upgradation of basic quantity of g-C_3N_4 was attributed to the reaction of metal halide between the active amine species of g-C_3N_4. Despite their low surface areas, under the same catalytic conditions, Zn-g-C_3N_4 catalysts demonstrated remarkably higher catalytic activity than other mesoporous carbon nitride materials.

Keywords: Carbon Nitride; Transesterification; Dimethyl Carbonate; Ethylene Carbonate

1. Introduction

During the past decade, owing to its reactive versatility and low toxicity, dimethyl carbonate (DMC) has attracted tremendous attention as one of the most important chemicals in numerous applications [1, 2]. DMC is an ideal additive for gasoline because of its higher oxygen content (53wt%), good blending octane, and rapid biodegradation [3, 4]. More significantly, DMC has been regarded as the most promising alternative to highly toxic phosgene and traditional dimethyl sulphate in carbonylation and methylation reactions [5-7], respectively. These merits enable DMC as a versatile and eco-friendly building block in modern chemistry. The conventional industrial routes to manufacture DMC, namely, phosgenation and oxidative carbonylation of methanol, involve high-risk compounds such as phosgene and CO [5, 8, 9]. Due to the increasing public attention towards the development of green and sustainable chemistry, much effort has been devoted to developing new approaches for the synthesis of DMC.

Among the several routes proposed, transesterification of cyclic carbonates (e.g. ethylene carbonates (EC) or propylene carbonate (PC)) with simple alcohols (e.g. CH_3OH or C_2H_5OH) has been considered as a clean and sustainable synthetic pathway for the production of DMC [10, 11] . Moreover, the co-products generated in the transesterification reactions, i.e. ethylene glycol (EG) and propylene glycol (PG), are also of commercial importance in the synthesis of polyester fibre and films [12]. A large number of catalysts, including basic metal oxides [6], alkali-metal hydroxides [13], anion-exchange resins [3], hydrotalcites [14], dawsonites [1], smectites [15], ceria-based materials [16, 17], etc, have been proposed for the transesterification reactions. To date, the most efficient catalysts reported for the processes have been considered as ionic liquids (ILs) [18, 19]. Unfortunately, the homogeneous IL catalysts suffer from intrinsic disadvantages in catalyst–product separation [20]. Although immobilization of the ILs onto porous siliceous materials could alleviate the difficulty [12, 21], the high cost of coupling agents and tedious preparation for the grafted ILs still remain as inevitable shortcomings for their wide applications. Very recently, nitrogen-based carbon materials [22-25] have demonstrated potential

application as base catalysts in various organic reactions; however, their catalytic activity was not satisfactory and meanwhile their application towards wider organocatalysis processes is being exploited.

Graphitic carbon nitride (g-CN) materials have recently emerged as fascinating and promising materials that are receiving worldwide attention. g-CN materials provide access to even wider range of applications than classical carbon materials in many fields including photocatalysis [26, 27], fuel cells [28, 29], gas storage [30, 31], and heterogeneous catalysis [32-34], etc. One significant note is that the incorporation of nitrogen atoms into carbon architecture endows g-CN materials with abundant basic sites in the forms of amine groups, etc, thereby enabling them as typical solid base catalysts [24, 35]. We previously reported the synthesis of mesoporous CN materials using mesoporous siliceous materials (i.e. MCF and FDU-12) as hard templates, and carbon tetrachloride plus ethylenediamine and dicyandiamide as precursors [36-39]. In the base-centred organocatalysis reactions, including Knoevenagel condensation [36, 39], transesterification of β-keto esters [38], and transesterification of EC to DMC [37], the synthesized mesoporous carbon nitride materials demonstrated potential catalytic activities.

However, in terms of catalyst preparation, such mesoporous catalysts were all based on nanocasting approaches [40, 41] which involved time-consuming detemplating procedure, and meanwhile the detemplating agents used (e.g. HF or NH_4HF_2) are volatile and/or hazardous [42, 43]. Secondly, besides etching silica templates, HF is also acidic, which could react with the basic sites of mesoporous g-CN materials (especially at the edges of graphitic sheets), thereafter sacrificing partial catalytic active sites and finally leading to a decline in catalytic activity [44]. In addition, the EC conversions in the abovementioned catalytic reactions were *ca*. 75%, relatively lower than the average value (~80%) achieved over other heterogeneously catalytic systems. In the continued exploitation of g-CN materials for practical applications towards the base catalysis, there is a definite demand to design a new and robust g-CN catalyst which can be simply prepared and afford a high-performance catalytic activity. In this contribution, we introduce a facile and

efficient preparation method for g-CN-based catalyst, namely Zn-g-C_3N_4. The sample only required a simple introduction of zinc halides into dicyandiamide (DCDA) and a following calcination. In the transesterification of EC to DMC, the Zn-g-C_3N_4 catalyst exhibited a superior catalytic yield of DMC, affording a maximum value up to 83%. Furthermore, the catalyst could be recycled for at least five runs without a remarkable loss in activity and also showed catalytic capability for the transesterification reactions of EC and other alcohols.

2. Experimental

2.1. Preparation of Zn-g-C_3N_4 materials

4 g of DCDA was added into 30 mL of ethanol containing zinc halide. The suspension was heated at 40 °C until remove of ethanol and formation of a white solid. The solid was then grounded, transferred into a closed crucible, and heated under air at 2 °C min^{-1} up to 550 °C and further treated for further 4 h. Finally, a powder with a yellow colour was obtained, and the mass yield in respect to the initial DCDA was *ca*. 50wt%. The resultant sample was labelled as *n*Zn-g-C_3N_4, where *n* represented the molar amount of Zn ($\times 10^{-4}$ mol) introduced. Unless otherwise specified, Zn-g-C_3N_4 was prepared using $ZnBr_2$ as a dopant and the amount of Zn was 2.1×10^{-4} mol. The actual loading amounts of Zn were measured by inductively coupled plasma atomic emission spectroscopy (ICP-AES, Varian Vista-AX). The detailed analytic experiments and the final values were summarized in **Table S1**. For instance, the actual content of Zn in 2.1Zn-g-C_3N_4 was *ca*. 0.92×10^{-4} mol $g_{catal.}^{-1}$.

2.2. Sample characterization

X-ray diffraction patterns were recorded with a Rigaku D/max 2500 PC X-ray diffractometer equipped with a graphite monochromator (40 kV, 40 mA) using Ni-filtered Cu-*K*α radiation (λ = 1.5418 Å).

Fourier transform infrared (FT-IR) spectra of the samples were collected in transmission mode from KBr pellets at room temperature on a Bruker Tensor 27 spectrometer with a resolution of 4 cm^{-1}, using 32 scans per spectrum in the region of 400–4000 cm^{-1}. The mass ratio of every sample to KBr was constant at 1:200.

X-ray photoelectron spectroscopy (XPS) measurements were performed using a

Perkin–Elmer PHI 5000C spectrometer working in the constant analyzer energy mode with Mg K_α radiation as the excitation source. The carbonaceous C 1s line (284.6 eV) was used as the reference to calibrate the binding energies (B.E.).

UV-Vis diffuse reflectance spectra (DRS) were recorded on a Shimizu UV-3600 spectrophotometer. $BaSO_4$ was used as a standard reference. Each sample was pressed into a thin tablet and tested under ambient conditions. The absorption spectrum was calculated from the reflectance data with Kubelka–Munk function.

Elementary analysis (EA) was performed with Elementar Vario EL III instrument to determine the carbon, nitrogen, hydrogen, and sulphur content of the samples.

CO_2 temperature-programmed desorption (CO_2-TPD) experiments were conducted using a Quantachrome ChemBET-3000 analyzer. A 200 mg of the sample was pretreated at 300 °C for 1 h in dry He flow (30 mL min^{-1}), cooled to 50 ℃, and then exposed to CO_2 for 0.5 h. After purging the sample with He for 0.5 h, the TPD data was recorded from 50 to 450 °C with a ramping rate of 10 ℃ min^{-1}.

2.3. Catalytic evaluation

The transesterification reactions of EC with CH_3OH were carried out in 80 mL stainless steel autoclave equipped with a magnetic stirrer. 25 mmol (1.7 mL) of EC and 250 mmol (10.1 mL) of CH_3OH were mixed well, followed by the introduction of 0.1 g of catalyst. The reactor was pressurized with CO_2 to 0.6 MPa and heated to 160 °C under stirring for several hours. After the reaction, the autoclave was cooled down in ice water and the mixture was centrifuged and analyzed by a GC equipped with a PEG-2000 capillary column coupled with a FID detector. The quantity of reagents and products are calculated by an area-normalization method. The carbon balance was 100±5%. In the transesterification of EC with CH_3OH, DMC and 2-hydroxyethyl methyl carbonate (HEMC) is the target molecule and by-product, respectively. The glycol is co-product. The conversion (Conv.) of EC and selectivity (Sel.) to DMC were calculated as follows:

$$\text{Conv.}\% = \frac{n_{\text{EC, fed}} - n_{\text{EC, uncoverted}}}{n_{\text{EC, fed}}} \quad , \quad \text{and} \quad \text{Sel.}\% = \frac{n_{\text{DMC}}}{n_{\text{EC, fed}} - n_{\text{EC, uncoverted}}} \quad .$$

The turnover frequency (TOF) value for each catalyst was calculated as follows:

$$\text{TOF}= \frac{m_{\text{EC,converted}}}{W_{\text{catal.}} \times t} = \frac{n_{\text{EC}} \times \text{Conv.\%(EC)} \times M_{\text{EC}}}{W_{\text{catal.}} \times t},$$

where n_{EC}, M_{EC}, t, and $W_{catal.}$ are the molar amount (mol), formula weight (88 g mol^{-1}) of EC, reaction time (h), and the mass of the catalyst (g), respectively.

3. Results and discussions

3.1. Structure characterization

XRD patterns of g-C_3N_4 and Zn-g-C_3N_4 materials are displayed in Fig. 1. Each sample represented two diffraction peaks at 2θ = 27.4 and 13.1 °. The primary peak with sharp intensity corresponded to the (002) planes (d = 0.325 nm), typical interplanar stacking structures of graphitic materials [45, 46]. The other minor peaks, corresponding to a distance of 0.675 nm, were indexed as (100) planes, i.e. the in-plane structural packing motifs [45, 47]. Compared with the pure g-C_3N_4, Zn-g-C_3N_4 samples demonstrated no obvious shift of (002) lines, suggesting that the graphitic stacking of g-C_3N_4 was essentially not affected by the introduction of Zn species. However, on the other hand, upon adding $ZnBr_2$, the overall intensity of diffraction peaks decreased, which has been also observed in the XRD patterns of g-C_3N_4 samples prepared using $ZnCl_2$ (Zn-g-C_3N_4-Cl) and ZnI_2 (Zn-g-C_3N_4-I) as dopants. This implied that the crystallinity of g-C_3N_4 materials decreased, and more edge defects generated [48] after the introduction of Zn elements.

The effect of metal incorporation on the electronic structure of g-C_3N_4 was investigated by means of UV-Vis DRS characterization. As shown in **Fig. 2**, the spectrum of g-C_3N_4 exhibited an intensive absorption peak in UV region, which was ascribed to the bandgap between HOMO and LUMO in the polymeric melon units of g-C_3N_4 [27, 28, 33]. After the introduction of Zn, the absorption edge of the samples was moved towards longer wavelengths. The shift probably originated from the d–p repulsion of the Zn 3d and N 2p orbits [49], suggesting a host–guest interaction between the Zn atoms and g-C_3N_4, similar to what have been witnessed in g-C_3N_4 supported VO [50] catalysts and $(Ga_{1-x}Zn_x)(N_{1-x}O_x)$ solid solution photocatalysts [51].

XPS technique was employed to analyze the chemical composition of g-C_3N_4 materials. The XPS survey (**Fig. 3**) manifested that the main components of g-C_3N_4

were carbon, nitrogen and oxygen elements. As far as the origin of the oxygen species, **Fig. S1** gives the fine O 1s spectra of both g-C_3N_4 and Zn-g-C_3N_4, and reveals a major peak located at *ca*. 533.6 eV, which is attributed to the –OH groups of water molecules [52], indicating that oxygen atoms came from the adsorbed water molecules on the surface of g-C_3N_4. Likewise, the Zn-g-C_3N_4 catalyst revealed similar spectrum, indicating that the overall chemical compositions on the surface of g-C_3N_4 materials had not changed. In addition to C, N, and O, the XPS surveys of the Zn-g-C_3N_4 sample also demonstrated the signal of Zn element with weak intensity centred at a B.E. = 1029 eV. By contrast, the residual Br element (Br 3p3: *ca*. 182 eV; 3d5: ca. 69 eV) has not been detected.

In order to further investigate the detailed chemical states of the above samples, deconvolution of N 1s spectra was performed. As presented in **Fig. 4**, the N 1s spectrum of g-C_3N_4 could be deconvoluted into four independent peaks, suggesting that there existed four types of N species with different bonding states on the surface of g-C_3N_4. The major peak with the strongest intensity located at 400.1 eV was attributed to the sp2-hybridized N atoms bonded with two C atoms (i.e. C=N–C) in the triazine rings [32]. The peak centred at 401.1 eV was assigned to the sp2-hybridized N atoms bonded with three atoms, i.e. C–N(–C)–C or C–N(–C)–H groups [53]. Such tertiary N atoms were key junctions that bridge tri-*s*-triazine units, thus forming the polymeric C_3N_4 sheets [33, 35]. More importantly, the sp2-hybrized tertiary N atoms have been considered as the essentially active sites in base-centred transesterification of β-keto esters [38] and cycloaddition of CO_2 [48]. The peak at 402.2 eV was associated with the sp3-hybridized N atoms located at the edges of C_3N_4 sheets, which were also regarded as uncondensed terminal amines (such as –NH_2) [32]. The sp3 N atoms contributed an apparent shoulder in the overall N 1s spectrum. Moreover, the last minute peaks yet with the highest BE value was due to the quaternary N species and/or charging effect [32].

For Zn-g-C_3N_4, the intensity of the shoulder of sp3 N species weakened obviously. Based on the peak areas calculated, the distributions of sp3 N (402.2 eV) and bridging N (401.1 eV) atoms in the case of the pure g-C_3N_4 sample were 16.4% and 17.8%,

respectively. By comparison, the corresponding values for two types of N species over Zn-g-C_3N_4 were 12.8% and 20.4%, respectively. On the other hand, the distributions for the other two N species (aromatic N atoms in the triazine rings and quaternary N atoms) showed no significant change, compared with those obtained over g-C_3N_4. In general, g-C_3N_4 material was synthesized through a series of self-condensation reactions from DCDA to g-C_3N_4 [44, 46]. Simultaneously, owing to the existence of plenty of amine species (especially –NH_2 and –NH– groups) at the edges of polymeric carbon nitride, the zinc halide reacted with the terminal amine species and generated hydrogen halides (e.g. HCl or HBr) and even ammonium halides (e.g. NH_4Br, **Scheme 1**). After the reaction, the positive Zn^{2+} cations were left in the g-C_3N_4 framework, and neutralized by negative charges on the nitrogen atoms [54]. Herein, it is of interest to probe the chemical state of Zn elements in the present Zn-g-C_3N_4 material. Considering this issue, we performed an additional XPS characterization for the Zn 2p spectrum of Zn-g-C_3N_4. The corresponding spectrum (**Fig. S2**) presents two peaks located at *ca*. 1022 and 1045 eV, corresponding to the signals of Zn 2p 3/2 and 2p 1/2, respectively. The positions of the two signals were similar to those values reported previously involving zinc halide (e.g. $ZnCl_2$) catalysts supported on other materials [55, 56], confirming that the state of Zn in Zn-g-C_3N_4 was ionic instead of metallic. In addition, the interaction between Zn^{2+} and g-C_3N_4 has been evidenced by the abovementioned UV-Vis spectra of Zn-g-C_3N_4 catalysts. Consequently, the concentration of the terminal amines declined while the bridging N atoms increased. Furthermore, EA information (**Table S1**) also indicated that the N and H (Note: the H element was mainly derived from the terminal sp3-hybrized primary and secondary amines located at the edges of graphitic sheets of g-C_3N_4 (**Scheme 1**), and trace water molecules adsorbed on the surface.) molar concentrations gained over Zn-doped g-C_3N_4 samples were lower than the corresponding data of the pure C_3N_4 material, inferring that the doping of Zn halides led to a notable decline in the population of amine species.

Another effect resulting from the reaction between g-C_3N_4 and zinc halides was variation in terms of basicity of the final Zn-g-C_3N_4 materials. In the previous work

involving g-C_3N_4-catalyzed NO decomposition, Zhu et al [54] prepared a series of metal-doped g-C_3N_4 catalysts using Zn and Au salts as dopants, and found that the introduction of metal species into the g-C_3N_4 framework successfully enhanced the catalytic activity of NO decomposition. They attributed the catalytic improvement to the increased overall Lewis basicity after the addition of metal species, which unfortunately, the hypothesis has not been characterized. Herein, to prove the variation in basicity of g-C_3N_4 before and after the introduction of Zn dopants, we used CO_2-TPD to analyze the basicity of g-C_3N_4 and Zn-g-C_3N_4 samples (**Fig. 5**). Each material showed a broad desorption peak in the range of 125–400 °C; such peak was attributed to the basic sites associated with chemical or even physical adsorption of acidic CO_2 molecules [57]. Based on desorption peak integrated, the density of the basic sites for the pure g-C_3N_4 was *ca*. 128 μmol CO_2 $g_{catal.}^{-1}$. After the introduction of 0.7×10^{-4} mol of $ZnBr_2$, the basic density reached *ca*. 157 μmol CO_2 $g_{catal.}^{-1}$. Additionally, as shown in **Fig. 5**, as the amounts of $ZnBr_2$ increased, the basic intensities obtained increased progressively. The finding in these CO_2-TPD profiles agreed well with the above hypothesis, further confirming that the overall quantity of basicity in g-C_3N_4 was elevated after the addition of $ZnBr_2$ as a dopant. It is interesting to note that, despite identical amount of Zn (2.1×10^{-4} mol), the basic quantity of Zn-g-C_3N_4-Cl was *ca*. 150 μmol CO_2 $g_{catal.}^{-1}$, slightly lower than that achieved over Zn-g-C_3N_4. This phenomenon could be explained by the leaving ability of halides. Since the leaving ability of Br^- is superior to that of Cl^-, during the reaction between Zn halide and g-C_3N_4 (**Scheme 1**), $ZnBr_2$ was more active than $ZnCl_2$, therefore possibly creating higher quantity of basic bridging N species.

3.2. Catalyst activity

Since g-C_3N_4 possessed abundant intrinsic basic sites in the forms of N-containing groups, in this study, we employed g-C_3N_4 as a solid catalyst in the transesterification of EC with CH_3OH. Initially, a blank experiment without any catalyst was carried out and the result showed that the obtained EC conversion was *ca*. 20% and the selectivity to the target DMC was 82.5%. The byproduct in the transesterification reaction of EC with CH_3OH was solely monoester, i.e.

2-hydroxyethyl methyl carbonate (HEMC) originated from the uncompleted transesterification of EC (discussed below). After the addition of 0.1 g of g-C_3N_4 (entry 1 of **Table 1**), the EC conversion and DMC selectivity increased slightly. In comparison, Zn-g-C_3N_4 catalysts exhibited prominent selectivities (>94%). Meanwhile, with the increase of the amounts of Zn from 0.7 to 2.1 × 10^{-4} mol, the catalytic conversions increased continuously while much higher amounts of Zn (entries 5–6) resulted in the decline of catalytic activities. Obviously, the incorporation of Zn into g-C_3N_4 promoted the catalytic activity in the transesterification of EC. Furthermore, it can be also found that the TOF value for each catalyst correlated well with its corresponding basic quantity measured by CO_2-TPD profiles (**Table 1**), thus further indicating that the transesterification of EC with CH_3OH in the presence of Zn-g-C_3N_4 materials were typical base-centred catalytic process and the basic quantity directly facilitated the final catalytic activity. It is worth noting that, besides the transesterification of EC with CH_3OH, the one-step esterification of CH_3OH with CO_2 is also a synthetic route for the manufacture of DMC [58, 59]. Since the reaction circumstance in this study contained CH_3OH and CO_2 and the reaction was conducted under a high pressure (0.6 MPa), to rule out a possible contribution of the direct esterification to final yield of DMC, a control test in the absence of EC was also conducted. The corresponding result (entry 7) showed that the DMC yield could be negligible, verifying that the obtained DMC was mainly derived from the transesterification of EC with CH_3OH.

EC is a cyclic diester; there exist two-step nucleophilic attacks (**Scheme S1**) in its transesterification. Therein, HEMC is the intermediate resulting from the first nucleophilic attack [60]. In this sense, the final catalytic activity and selectivity of the transesterification of EC is mostly dependent on the reaction conditions and basicity. **Fig. 6** depicts the influences of reaction temperature and time on the catalytic performances. Under the mild reaction temperature of 140 °C, the transesterification reaction of EC with CH_3OH only proceeded with a low EC conversion of 21%. Further increasing the temperatures, the conversions and selectivities improved gradually. As the temperature was raised from 155 to 160 °C, the catalytic reaction

underwent a significant increase in activity, affording a maximum DMC yield of 83.3%. Therefore, the high temperature of 160 °C was a critical temperature in the present catalytic conditions, which has been also observed in the transesterification reactions of EC catalyzed by other mesoporous CN materials [37]. On the other hand, the dependence of catalytic performances on the reaction time has been also found. As the reaction was prolonged, the conversion and selectivity increased monotonously in 1–4 h but levelled off after 4 h. This was because that the transesterification reaction reached its thermodynamic equilibrium, which has been also found in the transesterification reactions of EC catalyzed by other catalysts [10, 11, 21]. Given the above catalytic results, a temperature of 160 °C and a time of 4 h were chosen as optimal choices for the subsequent catalytic evaluation.

Another issue of practical importance for the examination of a heterogeneous catalyst is its reusability and reproducibility. In view of this point, a series of consecutive tests were performed over Zn-g-C_3N_4 in the transesterification of EC with CH_3OH. After each catalytic run, the catalyst was rinsed by CH_3OH for several times. The weight of the obtained dried catalyst revealed almost no obvious loss (<5wt%), in comparison with that acquired before the catalytic test. This meant that the Zn-g-C_3N_4 catalyst has not suffered leaching problem during the catalytic reaction and the following washing procedures. More importantly, as shown in **Fig. 7**, after five repetitious runs, no apparent decline of the conversion or selectivity has been detected, indicating that the heterogeneous catalyst was quite stable for the transesterification reactions.

Besides $ZnBr_2$, we also examined the catalytic performances of other two Zn-g-C_3N_4 materials prepared using $ZnCl_2$ and ZnI_2 as dopants. As listed in **Table 2**, under the same reaction conditions, Zn-g-C_3N_4-Cl also gave a high EC conversion of 73.3%, yet slightly lower than that offered by Zn-g-C_3N_4. The gap in catalytic activity could be ascribed to the difference between their basic quantities of the two catalysts. Because the transesterification reaction of EC proceeded in the presence of the g-C_3N_4 material as a solid base catalyst (**Scheme S1**), high basic intensity favoured the catalytic process. In this sense, it is reasonable Zn-g-C_3N_4 with higher basic intensity

(**Fig. 5**) presented superior activity to Zn-g-C_3N_4-Cl. As for Zn-g-C_3N_4-I, since the leaving ability of I^- was stronger than that of Br^-, in light of this rule, it was expected that Zn-g-C_3N_4-I would exhibit a higher activity than Zn-g-C_3N_4. By contrary, the obtained EC conversion over Zn-g-C_3N_4-I was the lowest one. We surmise that the result may be associated with intrinsic chemical property of ZnI_2. Unlike $ZnCl_2$ or $ZnBr_2$, ZnI_2 itself is liable to react with H_2O and O_2 under ambient conditions, and then transferred into ZnO and I_2. Consequently, the actual amount of ZnI_2 reacting with g-C_3N_4 was much lower than the nominal value, therein deteriorating the basic intensity of the final Zn-g-C_3N_4-I sample.

In order to verify the basic improvement of g-C_3N_4 resulting from the introduction of metal halides, several compounds, including $FeCl_3$, $CuCl_2$, $NiCl_2$ and $CoCl_2$, were also utilized for the synthesis of metal-doped g-C_3N_4 composites. As expected, all the doped g-C_3N_4 composites (entries 4–8, **Table 2**) demonstrated relatively high EC conversions (> 70%) for transesterification of EC with CH_3OH, together with excellent selectivities to the desired DMC. In addition to the transesterification of EC with CH_3OH, the reactions with C_2H_5OH and *n*-C_3H_7OH have been also performed over the Zn-g-C_3N_4 catalyst (entries 9 and 10, **Table 2**). The results manifested that Zn-g-C_3N_4 could catalyze the transesterification of EC with other various alcohols; the order of catalytic activity was as follows: CH_3OH > C_2H_5OH > *n*-C_3H_7OH. In our previous work [37], we have proposed a possible reaction mechanism of the transesterification of EC catalyzed by CN materials (**Scheme S1**). Wherein, the terminal or bridging amines species, as typical bases, were considered as the catalytically active sites. The alcohol (R–OH) was activated by active N atoms via a hydrogen bond, thus generating RO^- anion (**Step 1**). As a nucleophile, the as-produced RO^- attacked the carbonyl C of EC, and yields $CH_3O–CO–O–CH_2CH_2O^-$ and CH_3OH (**Step 2**). Afterwards, the two molecules underwent a proton exchange (**Step 3**), followed by a second nucleophilic attack of RO^- (**Step 4**) and proton exchange (**Step 5**). In **Step 2**, the nucleophilic ability directly determined the reaction activity. Given this point, it is reasonable that, under the same reaction conditions, CH_3OH showed the highest catalytic activity whereas the DMC

yield received in the reaction with *n*-C_3H_7OH was the lowest one.

Table 3 summaries the catalytic performances of various CN catalysts in the transesterification reactions of EC. Both mp-C_3N_4 and CN-MCF were mesoporous CN materials prepared via nanocasting methods, which were fabricated using cyanamide, and carbon tetrachloride plus ethylenediamine as precursors, respectively. Under the same catalytic conditions, the two mesoporous catalysts demonstrated EC conversions above 75%. Undoubtedly, the high catalytic activities were mainly derived from their high surface areas and rich porosity. Taking into account their textual parameters, the activity per surface area for mp-C_3N_4 and CN-MCF were 0.68, and 0.46 $mmol_{EC}$ m^{-2}, respectively. In sharp contrast, the value achieved over Zn-g-C_3N_4 was as high as 19.14 $mmol_{EC}$ m^{-2}. Indeed, as shown in CO_2-TPD profiles, the desorption peaks of mp-C_3N_4 and CN-MCF were located in the range of 170–180 °C (**Fig. S3**), appreciably lower than the peak position revealed by Zn-g-C_3N_4 (**Fig. 5**). The comparison strongly verified that the catalytic activities of the three CN catalysts correlate well with their basic intensities. As mentioned above, during their preparation procedures, such mesoporous CN materials demanded a detemplating process, wherein HF or NH_4HF_2 was applied as an etching agent. Under this acidic circumstance, the original abundant basic N-containing species were inevitably partly sacrificed, thereafter resulting in an undesired degradation of the whole basicity in the final CN samples. By contrast, in this work, Zn-g-C_3N_4 was manufactured only by a facile mixing and calcination. In spite of low textual parameters, the inherent basic sites of g-C_3N_4 have been well retained. At this juncture, combining its simple, eco-benign preparation and high catalytic performances, we anticipate that the Zn-g-C_3N_4, or other transition-metal-doped g-C_3N_4 material, would emerge as a new heterogeneous catalyst for the transesterification of EC to DMC, or even wider base-centred organocatalysis reactions.

4. Conclusion

In conclusion, a cheap and convenient approach for the fabrication of Zn-doped g-C_3N_4 materials for the catalytic transesterification of EC to DMC has been reported. The dopants, Zn or other metal-transition halides were speculated to react with the

terminal uncondensed amines species located at the graphitic edges of g-C_3N_4, thus generating hydrogen and/or ammonium halides and meanwhile creating a possible interaction between metal and g-C_3N_4. The introduction of Zn or other metal species leaded to the promotion of the overall basic quantity of g-C_3N_4. In the transesterification reactions of EC, the Zn-doped g-C_3N_4 catalysts revealed higher EC conversions than the pristine g-C_3N_4 sample, affording a maximum DMC yield of 83.3%. The heterogeneous catalysts could be reused at least for five times without any significant loss in catalytic activity. Additionally, a wide range of transition-metal halides could be applied as dopants for g-C_3N_4, and the resultant catalytic EC conversions were above 70%. Compared with other mesoporous CN catalysts, notwithstanding its lower textual parameters, the doped g-C_3N_4 catalysts exhibited much higher catalytic activity.

Acknowledgments

This work was supported by National Natural Science Foundation of China (21203014), Open Foundation of Jiangsu Key Laboratory of Fine Petrochemical Engineering (KF1201), Jiangsu Key Laboratory of Advanced Catalytic Materials and Technology (BM2012110), and the Project Funded by the Priority Academic Program Development of Jiangsu Higher Education Institutions.

References:

[1] G. Stoica, S. Abelló, J. Pérez-Ramírez, ChemSusChem 2 (2009) 301-304.

[2] M. Sankar, S. Satav, P. Manikandan, ChemSusChem 3 (2010) 575-578.

[3] S.M. Dhuri, V.V. Mahajani, J. Chem. Technol. Biotechnol. 81 (2006) 62-69.

[4] H. Abimanyu, B.S. Ahn, C.S. Kim, K.S. Yoo, Ind. Eng. Chem. Res. 46 (2007) 7936-7941.

[5] B.M. Bhanage, S.-I. Fujita, Y. He, Y. Ikushima, M. Shirai, K. Torii, M. Arai, Catal. Lett. 83 (2002) 137-141.

[6] L. Wang, Y. Wang, S. Liu, L. Lu, X. Ma, Y. Deng, Catal. Commun. 16 (2011) 45-49.

[7] M. Wang, H. Wang, N. Zhao, Wei, Y. Sun, Ind. Eng. Chem. Res. 46 (2007) 2683-2687.

[8] M.M. Dharman, H.-Y. Ju, H.-L. Shim, M.-K. Lee, K.-H. Kim, D.-W. Park, J. Mol. Catal. A 303 (2009) 96-101.

[9] Y. Ding, A. Kong, H. Zhang, H. Shen, Z. Sun, S.D. Huang, Y. Shan, Appl. Catal. A 455 (2013) 58-64.

[10] T. Wei, M. Wang, W. Wei, Y. Sun, B. Zhong, Green Chem. 5 (2003) 343-346.

[11] Z.-Z. Yang, L.-N. He, X.-Y. Dou, S. Chanfreau, Tetrahedron Lett. 51 (2010) 2931-2934.

[12] J. Xu, H.-T. Wu, C.-M. Ma, B. Xue, Y.-X. Li, Y. Cao, Appl. Catal. A 464-465 (2013) 357-363.

[13] M.S. Han, B.G. Lee, B.S. Ahn, K.Y. Park, S.I. Hong, React. Kinet. Catal. Lett. 73 (2001) 33-38.

[14] Y. Watanabe, T. Tatsumi, Micropor. Mesopor. Mater. 22 (1998) 399-407.

[15] S.-I. Fujita, B.M. Bhanage, D. Aoki, Y. Ochiai, N. Iwasa, M. Arai, Appl. Catal. A 313 (2006) 151-159.

[16] J. Xu, K.-Z. Long, W. Fei, B. Xue, Y.-X. Li, Y. Cao, Appl. Catal. A 484 (2014) 1-7.

[17] T.-T. Li, L.-B. Sun, L. Gong, X.-Y. Liu, X.-Q. Liu, J. Mol. Catal. A 352 (2012) 38-44.

[18] J.-Q. Wang, J. Sun, W.-G. Cheng, C.-Y. Shi, K. Dong, X.-P. Zhang, S.-J. Zhang, Catal. Sci. Technol. 2 (2012) 600-605.

[19] H.Y. Ju, M.D. Manju, D.W. Park, Y. Choe, S.W. Park, React. Kinet. Catal. Lett. 90 (2007) 3-9.

[20] M.H. Valkenberg, C. deCastro, W.F. Holderich, Green Chem. 4 (2002) 88-93.

[21] D.-W. Kim, D.-O. Lim, D.-H. Cho, J.-C. Koh, D.-W. Park, Catal. Today 164 (2011) 556-560.

[22] L. Wang, L. Wang, H. Jin, N. Bing, Catal. Commun. 15 (2011) 78-81.

[23] N. Kan-Nari, S. Okamura, S.-I. Fujita, J.-I. Ozaki, M. Arai, Adv. Synth. Catal. 352 (2010) 1476-1484.

[24] X. Jin, V.V. Balasubramanian, S.T. Selvan, D.P. Sawant, M.A. Chari, G.Q. Lu, A. Vinu, Angew. Chem. Int. Ed. 48 (2009) 7884-7887.

[25] S. van Dommele, K.P. de Jong, J.H. Bitter, Chem. Commun. (2006) 4859-4861.

[26] F. Su, S.C. Mathew, G. Lipner, X. Fu, M. Antonietti, S. Blechert, X. Wang, J. Am. Chem. Soc. 132 (2010) 16299-16301.

[27] X. Wang, K. Maeda, A. Thomas, K. Takanabe, Nature Mater. 8 (2009) 76-80.

[28] Y. Zheng, J. Liu, J. Liang, M. Jaroniec, S.Z. Qiao, Energy Environ. Sci. 5 (2012) 6717-6731.

[29] Y. Zheng, Y. Jiao, J. Chen, J. Liu, J. Liang, A. Du, W. Zhang, Z. Zhu, S.C. Smith, M. Jaroniec, G. Lu, S. Qiao, J. Am. Chem. Soc. 133 (2011) 20116-20119.

[30] Q. Li, J. Yang, D. Feng, Z. Wu, Q. Wu, S.S. Park, C.-S. Ha, D. Zhao, Nano Res. 3 (2010) 632-642.

[31] S.S. Park, S.-W. Chu, C. Xue, D. Zhao, C.-S. Ha, J. Mater. Chem. 21 (2011) 10801-10807.

[32] A. Thomas, A. Fischer, F. Goettmann, M. Antonietti, J.-O. Müller, R. Schlögl, J.M. Carlsson, J. Mater. Chem. 18 (2008) 4893-4908.

[33] Y. Wang, X. Wang, M. Antonietti, Angew. Chem. Int. Ed. 51 (2012) 68-89.

[34] M.B. Ansari, B.-H. Min, Y.-H. Mo, S.-E. Park, Green Chem. 13 (2011) 1416-1421.

[35] J. Zhu, P. Xiao, H. Li, S.A.C. Carabineiro, ACS Appl. Mater. Inter. 6 (2014)

16449-16465.

[36] J. Xu, K. Shen, B. Xue, Y.-X. Li, Y. Cao, Catal. Lett. 143 (2013) 600-609.

[37] J. Xu, K.-Z. Long, T. Chen, B. Xue, Y.-X. Li, Y. Cao, Catal. Sci. Technol. 3 (2013) 3192-3199.

[38] J. Xu, F. Wu, H.-T. Wu, B. Xue, Y.-X. Li, Y. Cao, Micropor. Mesopor. Mater. 198 (2014) 223-229.

[39] J. Xu, T. Chen, Q. Jiang, Y.-X. Li, Chem. -Asian J. 9 (2014) 3269-3277.

[40] H. Yan, Chem. Commun. 48 (2012) 3430-3432.

[41] J. Xu, H.-T. Wu, X. Wang, B. Xue, Y.-X. Li, Y. Cao, Phys. Chem. Chem. Phys. 15 (2013) 4510-4517.

[42] Y. Wang, X. Wang, M. Antonietti, Y. Zhang, ChemSusChem 3 (2010) 435-439.

[43] J. Xu, Y. Wang, Y. Zhu, Langmuir 29 (2013) 10566-10572.

[44] Z. Huang, F. Li, B. Chen, T. Lu, Y. Yuan, G. Yuan, Appl. Catal. B 136 (2013) 269-277.

[45] F. Goettmann, A. Fischer, M. Antonietti, A. Thomas, Angew. Chem. Int. Ed. 45 (2006) 4467-4471.

[46] M.J. Bojdys, J.-O. Müller, M. Antonietti, A. Thomas, Chem. -Eur. J. 14 (2008) 8177-8182.

[47] S.C. Lee, H.O. Lintang, L. Yuliati, Chem. -Asian J. 7 (2012) 2139.

[48] Q. Su, J. Sun, J. Wang, Z. Yang, W. Cheng, S. Zhang, Catal. Sci. Technol. 4 (2014) 1136-1138.

[49] X. Wang, X. Chen, A. Thomas, X. Fu, M. Antonietti, Adv. Mater. 21 (2009) 1609-1612.

[50] J. Xu, Q. Jiang, T. Chen, F. Wu, Y.-X. Li, Catal. Sci. Technol. DOI: 10.1039/C4CY01373E (2015).

[51] K. Maeda, K. Domen, J. Phys. Chem. C 111 (2007) 7851-7861.

[52] Q. Li, R. Jiang, Y. Dou, Z. Wu, T. Huang, D. Feng, J. Yang, A. Yu, D. Zhao, Carbon 49 (2011) 1248-1257.

[53] E. Raymundo-Piñero, D. Cazorla-Amorós, A. Linares-Solano, J. Find, U. Wild, R. Schlögl, Carbon 40 (2002) 597-608.

[54] J. Zhu, Y. Wei, W. Chen, Z. Zhao, A. Thomas, Chem. Commun. 46 (2010) 6965-6965.

[55] S.K. Pillai, S. Hamoudi, K. Belkacemi, Appl. Catal. A 455 (2013) 155-163.

[56] S.A. Schmidt, N. Kumar, A. Shchukarev, K. Eränen, J.-P. Mikkola, D.Y. Murzin, T. Salmi, Appl. Catal. A 468 (2013) 120-134.

[57] S.N. Talapaneni, S. Anandan, G.P. Mane, C. Anand, D.S. Dhawale, S. Varghese, A. Mano, T. Mori, A. Vinu, J. Mater. Chem. 22 (2012) 9831-9840.

[58] Y. Yoshida, Y. Arai, S. Kado, K. Kunimori, K. Tomishige, Catal. Today 115 (2006) 95-101.

[59] M. Honda, M. Tamura, Y. Nakagawa, K. Tomishige, Catal. Sci. Technol. 4 (2014) 2830-2845.

[60] Y.-J. Fang, W.-D. Xiao, Sep. Purif. Technol. 34 (2004) 255-263.

Figure Captions

Fig. 1 XRD patterns of g-C_3N_4 (a), 0.7Zn-g-C_3N_4 (b), 1.4 Zn-g-C_3N_4 (c), 2.1Zn-g-C_3N_4 (d), Zn-g-C_3N_4-Cl (e), and Zn-g-C_3N_4-I (f) materials.

Fig. 2 UV-Vis spectra of g-C_3N_4 and Zn-g-C_3N_4 materials. Arrow direction: g-C_3N_4, 1.4Zn-g-C_3N_4, 2.1Zn-g-C_3N_4, 2.8Zn-g-C_3N_4, Zn-g-C_3N_4-Cl, and Zn-g-C_3N_4-I.

Fig. 3 XPS surveys of g-C_3N_4 (a), Zn-g-C_3N_4 (b) materials.

Fig. 4 N1s spectra of g-C_3N_4 (A) and 2.1Zn-g-C_3N_4 (B) samples.

Fig. 5 CO_2-TPD profiles of g-C_3N_4 (a), 0.7Zn-g-C_3N_4 (b), 1.4Zn-g-C_3N_4 (c), 2.1Zn-g-C_3N_4 (d), and Zn-g-C_3N_4-Cl (e) catalysts.

Fig. 6 Effect of reaction temperature (A) and time (B) on the transesterification over Zn-g-C_3N_4. Reaction conditions: 250 mmol of CH_3OH, 25 mmol of EC, and $W_{catal.}$ = 0.1 g.

Fig. 7 Evolution of transesterification reactions of EC with CH_3OH during five consecutive runs in the presence of Zn-g-C_3N_4. Reaction condition: 250 mmol of CH_3OH, 25 mmol of EC, T = 160 °C, $W_{catal.}$ = 0.1 g, and t = 4 h.

Fig. 1

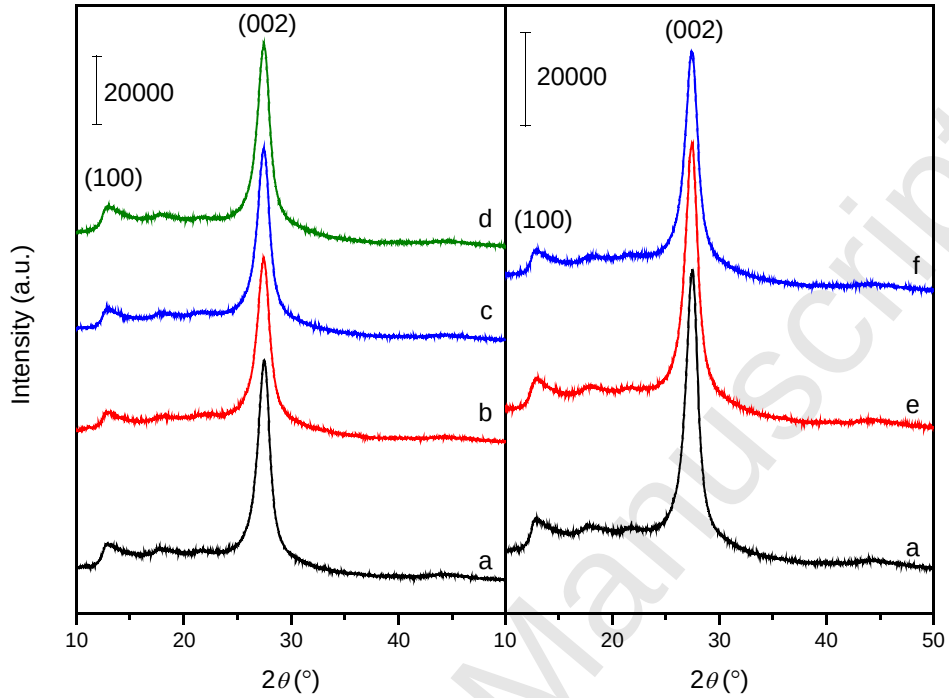

Fig. 2

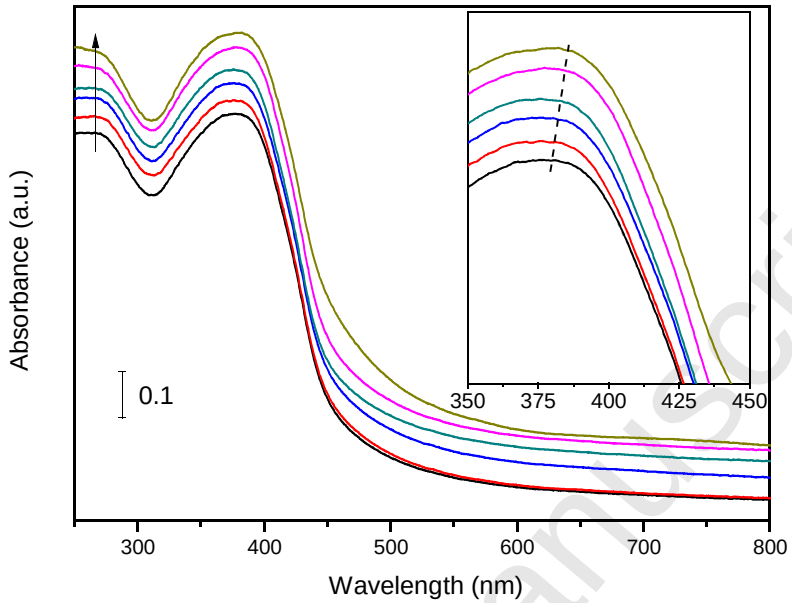

Fig. 3

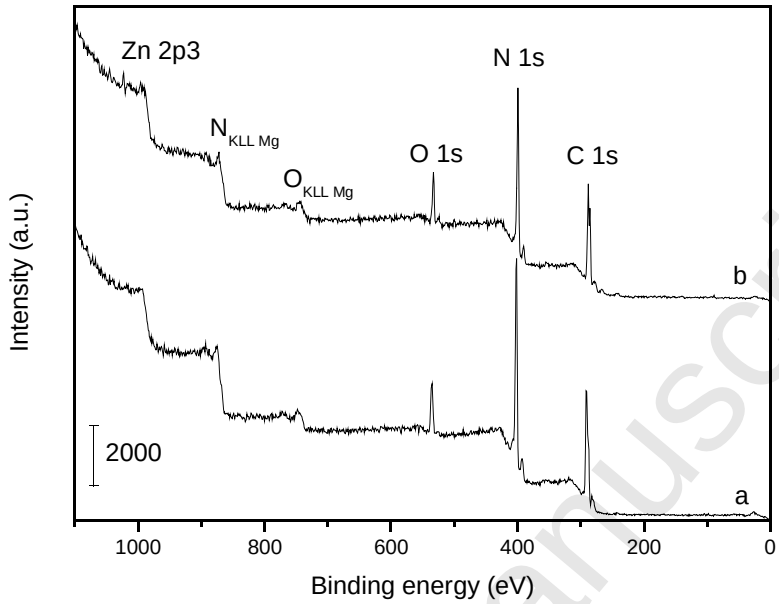

Fig. 4

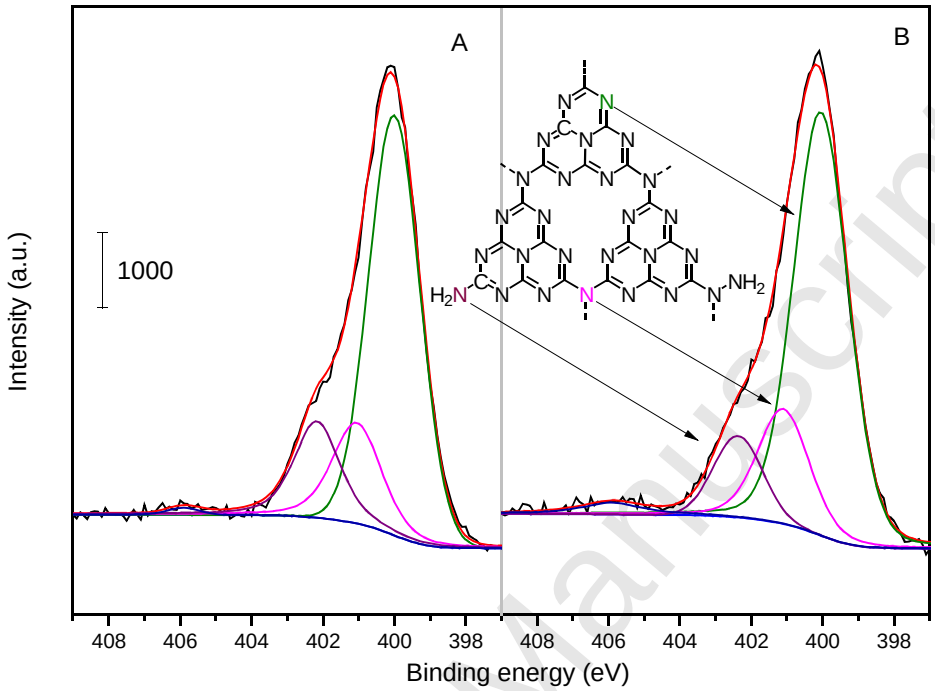

Fig. 5

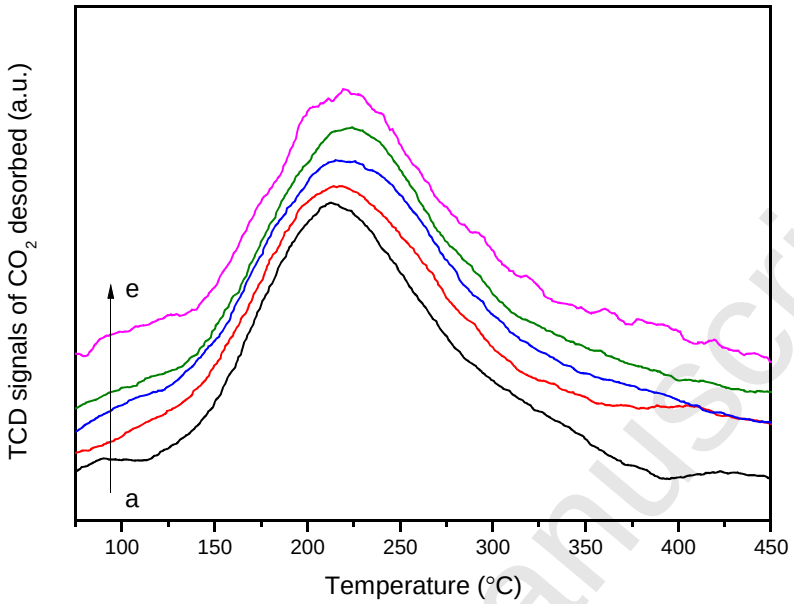

Fig. 6

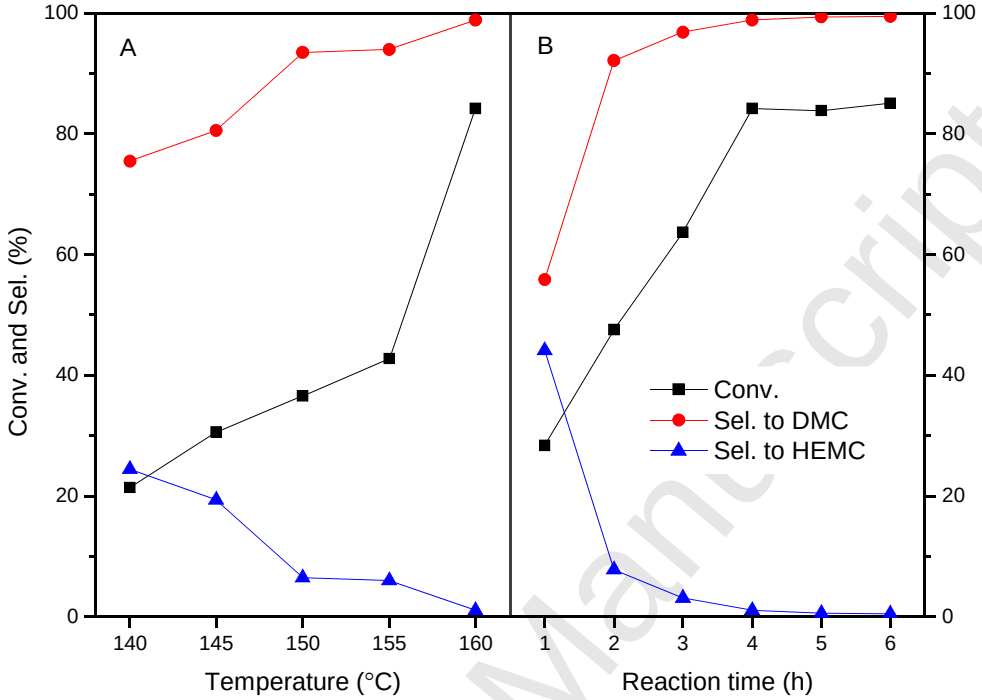

Fig. 7

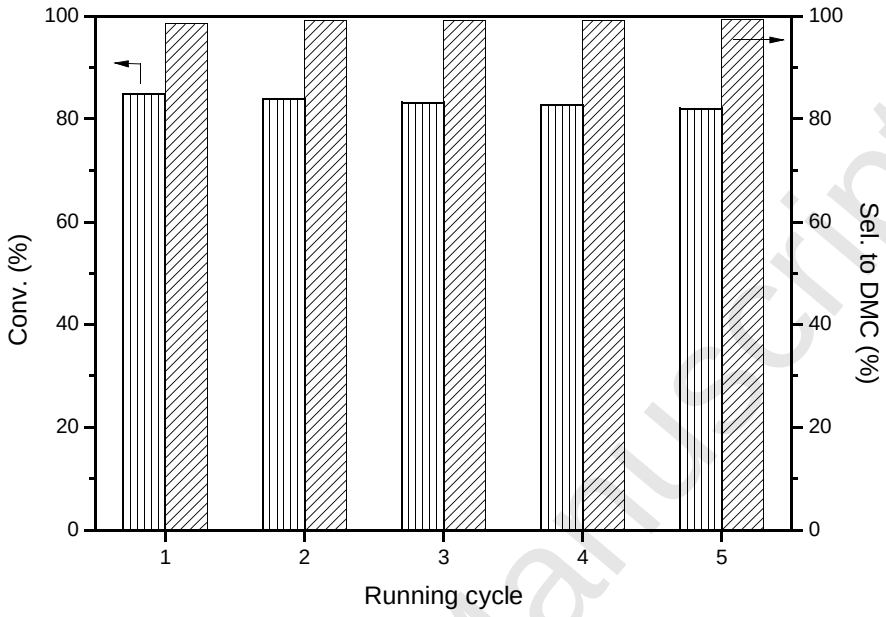

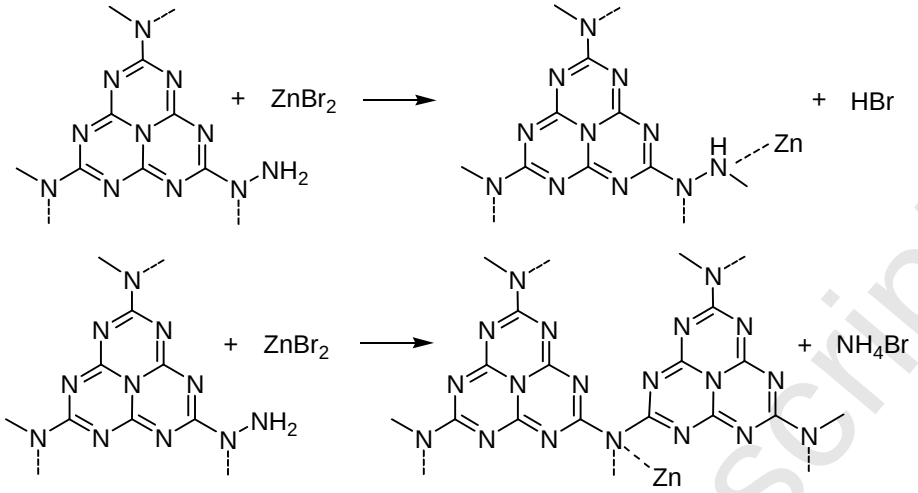

Scheme 1 A possible reaction between g-C_3N_4 and $ZnBr_2$.

Table 1 Catalytic performances of g-C_3N_4 and Zn-g-C_3N_4 catalysts in transesterification reactions of EC with CH_3OH.

Entry	Catalyst	Conv. (%)	Sel. (%)	Yield (%)	TOF (g_{EC} $g_{catal.}^{-1}$ h^{-1})	Basicity (μmol CO_2 $g_{catal.}^{-1}$) [c]
1 [a]	g-C_3N_4	30.8	84.4	26.0	1.69	128
2 [a]	0.7Zn-g-C_3N_4	46.6	94.3	43.9	2.56	136
3 [a]	1.4Zn-g-C_3N_4	65.4	94.7	61.9	3.60	145
4 [a]	2.1Zn-g-C_3N_4	84.2	98.9	83.3	4.63	157
5 [a]	2.8Zn-g-C_3N_4	64.2	92.1	59.1	3.53	140
6 [a]	3.5Zn-g-C_3N_4	66.6	98.2	65.4	3.66\	–
7 [b]	2.1Zn-g-C_3N_4	–	–	<1	–	157

[a] 250 mmol of CH_3OH, 25 mmol of EC, T = 160 °C, $W_{catal.}$ = 0.1 g, 0.6 MPa of CO_2, and t = 4 h. [b] 250 mmol of CH_3OH, T = 160 °C, $W_{catal.}$ = 0.1 g, 0.6 MPa of CO_2, and t = 4 h. [c] Calculated according to the CO_2-TPD profiles.

Table 2 Catalytic results of transesterification reactions catalyzed by various metal-doped g-C_3N_4 catalysts using various halide dopants [a].

Entry	Dopant	*t* (h)	Conv. (%)	Sel. (%)	Yield (%)
1	$ZnCl_2$ [b]	4	73.3	98.5	72.2
2	$ZnBr_2$ [b]	4	84.2	98.9	83.3
3	ZnI_2 [b]	4	64.0	97.9	62.7
4	$FeCl_3$ [b]	4	42.1	96.2	40.5
5	$FeCl_3$ [b]	6	73.5	98.7	72.5
6	$CuCl_2$ [b]	6	75.5	98.6	74.4
7	$NiCl_2$ [b]	6	73.1	98.7	72.1
8	$CoCl_2$ [b]	6	74.0	97.3	72.0
9	$ZnBr_2$ [c]	4	57.4	70.5	40.5
10	$ZnBr_2$ [d]	4	28.0	63.8	17.9

[a] Each molar amount of the metal halide was fixed as 2.1×10^{-4} mol. Reaction conditions: 250 mmol of alcohol, 25 mmol of EC, T = 160 °C, and $W_{catal.}$ = 0.1 g. [b] CH_3OH. [c] C_2H_5OH. [d] *n*-C_3H_7OH.

Table 3 Comparison of catalytic performances over various CN catalysts [a].

Catalyst	S_{BET} (m^2 g^{-1})	V_p (cm^3 g^{-1})	Conv. (%)	Sel. (%)	Activity per surface area ($mmol_{EC}$ m^{-2}) [d]
g-C_3N_4 [b]	17	0.11	30.8	84.4	4.53
Zn-g-C_3N_4 [b]	11	0.05	84.2	98.9	19.14
mp-C_3N_4 [b]	285	0.92	77.7	96.4	0.68
CN-MCF [c] [37]	432	0.84	78.6	99.0	0.46

[a] Reaction conditions: 250 mmol of CH_3OH, 25 mmol of EC, T = 160 °C, and $W_{catal.}$ = 0.1 g. [b] t = 4 h. [c] t = 6 h. [d] Calculated as follows: $n_{EC} \times Conv./(S_{BET} \times W_{catal.})$, where n_{EC} is the molar amount of EC fed.